Synoptic Mapping of North Polar Sea Ice Melt/Freeze and Landscape Freeze/Thaw State: Assessment of the North Polar Climate System Using Microwave Remote Sensing and Modeling

- Cassandra Calderella, Nicholas Steiner, Kyle McDonald, Department of Earth and Atmospheric Sciences NOAA CREST, and Environmental Crossroads Initiative, City College of New York, New York, NY, U.S.A.
- Pamela Posey, Naval Research Laboratory, Stennis Space Center, Mississippi, U.S.A
- Benjamin Holt, Jet Propulsion Laboratory, California Institute of Technology, Pasadena, California, U.S.A

ABSTRACT

The effect of climate change on Earth's high latitudes has become apparent. This circumpolar region, from 60°N to 90°N, is being increasingly influenced by warming temperatures, with noticeable consequences on Arctic sea ice cover and boreal/ Arctic terrestrial biomes. With warming temperatures occurring and the subsequent melting of the sea ice and increasing non-frozen seasons over the terrestrial biomes, it is important to understand past, present, and future condition of this region and associated feedbacks to global climate. We apply time series microwave scatterometer data to examine seasonal transitions across this domain. We compare with model output from the Arctic Cap Nowcast/Forecast System (ACNFS) to examine commonalities in modeled fields and remote sensing observations of the sea ice, examining modeled air temperatures and the freeze/melt potential. Backscatter data utilized in this effort include multi-year observations from the Advanced Scatterometer (ASCAT) and the SeaWinds-on-QuikSCAT. These two remote sensing datasets help elucidate the land-sea ice interaction that may contribute to systematic feedbacks, with implications to coupling with the global climate system.

BACKGROUND

ACNFS is a fully coupled data assimilative ice/ocean model run daily at the Navy Oceanographic Office. ACNFS provides modeled information of ice condition for all ice-covered areas northward of 40 degrees. The system provides ~50 products, including ice thickness, ice concentration, ice drift, air temperature (10 m) and the freeze/melt potential of the sea ice.

ASCAT is a C-band microwave scatterometer launched in 2006 by the European Organization for the Exploration of Meteorological Satellites (EUMETSAT). ASCAT uses a wide-swath fan-beam antenna design to measure C-band VV-polarized backscatter providing daily synoptic observations of the high latitudes.

SeaWinds-on-QuikSCAT is a Ku-band microwave scatterometer launched in 1999 by the National Aeronautics and Space Administration (NASA). QuikSCAT utilized a scanning dish antenna design to provide HH- and VV-polarized backscatter measurement at incidence angles of 46 and 54 degrees, respectively. Although QuikSCAT experienced a sensor loss in 2009 and has not provided full mapping capabilities since, the data that it has collected can be used to provide daily mappings of the high latitudes from 2000-2009.

OBJECTIVES

Goals and objectives of this research include:

Development of a consistent remote sensing-based integrated characterization of land surface freeze/thaw and sea ice melt/ freeze status from QuikSCAT and ASCAT for the circumpolar high latitudes.

Improved characterization of the seasonal sea ice properties for the north polar region using the ACNFS model informed by remote sensing data, combining computer modeling and satellite scatterometer datasets.

Validation of model-based and remote sensing based characterizations of sea ice and land surface processes with in situ dataset from ground stations and ocean buoys.

Operationalization of a sea ice monitoring and characterization system using data from NASA's new Soil Moisture Active-Passive (SMAP) mission.

Figure 1. A map showing my chosen ground station locations, as well as three points over the Beaufort Sea and the Arctic Ocean that I will also study.

PRIOR WORK

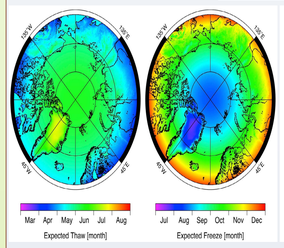

Figure 2. Expected seasonal freeze-thaw transition from cost functions accounting latitude and elevation retrieved from an internal climatology.

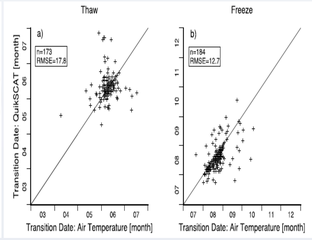

Figure 3. Scatter of transition from QuikSCAT and surface air temperature at sea between 1999 and 2009. The box on each plot surface contains the measurement quantity and root mean square error in days.

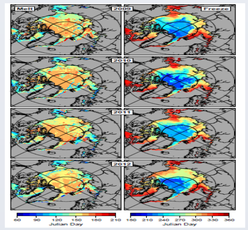

Figure 4. Seasonal melt (left column) and freeze (right column) transitions in Julian Day retrieved from ASCAT–SIC-constrained a posteriori transitions—for the years 2009-2012. The scale was chosen to clearly see outliers.

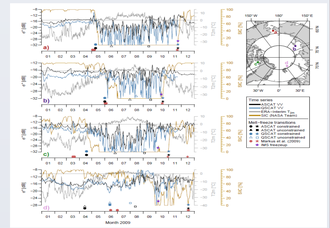

Figure 5. As Figs. 1 and 2, but for sites in areas in which the temporal evolution of σ° is more complex. The thresholds distinguishing MYI from FYI are excluded. Also, no confirmation with SAR imagery was performed for these sites. However, the algorithm estimates FYI coverage at all these sites from both QSCAT and ASCAT data.

NAVY MODEL DATA (ACNFS)

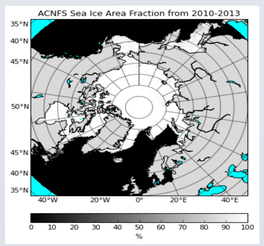

Figure 6. Map of sea ice concentration over the Arctic Ocean from 2010 to 2013.

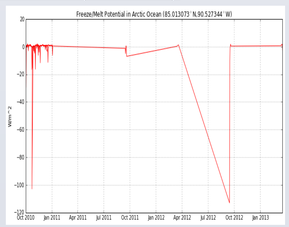

Figure 7. Time series of freeze/melt potential over the Arctic Ocean from 2010 to 2013. The sea ice melting period appears to take place most prominently in the spring seasons, such as April 2012, while the sea ice formation period would occur in the autumn months, such as October 2012. Values above zero indicate freezing, and values below zero indicate melting.

AMSR-E DATA

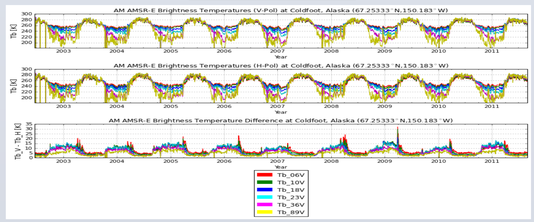

Figure 8. Time series of AMSR-E brightness temperatures and polarization differences measured over Coldfoot, Alaska, from 2002-2011.

SCATTEROMETER DATA

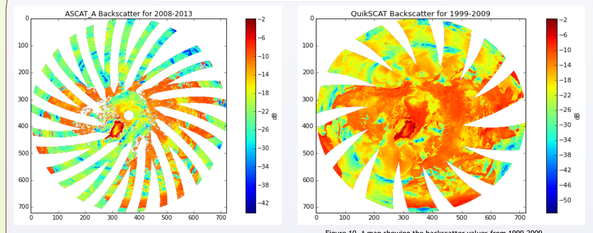

Figure 9. A map showing the backscatter values from 2008-2013 taken by ASCAT.

Figure 10. A map showing the backscatter values from 1999-2009 taken by QuikSCAT.

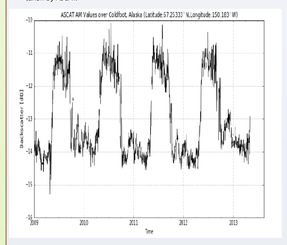

Figure 11. A chart showing the ASCAT backscatter values vs. time from 2008 to 2013 in Coldfoot, Alaska.

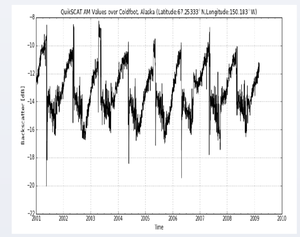

Figure 12. A chart showing the QuikSCAT backscatter values vs. time from 1999 to 2009 in Coldfoot, Alaska.

Freeze/Thaw Detection – Continuous Wavelet Transform

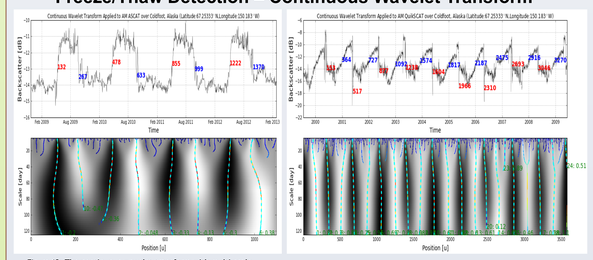

Figure 13. **The continuous wavelet transform with multi-scale analysis is used to localize transitions in observed backscatter caused by freeze/thaw and snowmelt processes** . Soil freeze and thaw seasonality at the Coldfoot SnoTel Station (67.253° N, -150.183° E) is observed as yearly positive and negative transitions in theco-localized backscatter from the C-Band Scatterometer, ASCAT(**top**). The timings of these transitions are estimated using a continuous wavelet transform (CWT), as illustrated in (**bottom**). Here the CWT acts as a differential operator where negative transitions result in positive maxima (***Julian days in red on the top graph***) and negative transitions have negative maxima (***Julian days in red on the top graph***) in transform space. Maxima positions are used to define seasonal F/ T timing.

Figure 14. Similarly, thaw or snowmelt timings can be observed in backscatter from the Ku-Band Scatterometer, QuikSCAT, as abrupt negative transitions. These transitions produce negative valued maxima in the CWT transformed data-record (Julian days in red on top graph).

VALIDATION OF IN SITU DATA

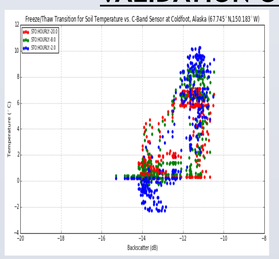

Figure 15. A chart showing the SNOTEL Soil Temperatures at various depths vs. backscatter for ASCAT in the year 2009.

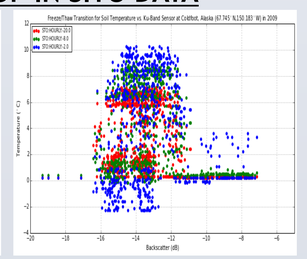

Figure 16. A chart showing the SNOTEL Soil Temperatures at various depths vs. backscatter for QuikSCAT in the year 2009.

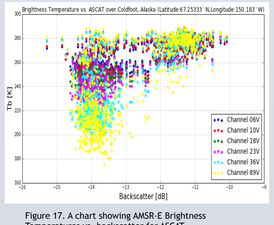

Figure 17. A chart showing AMSR-E Brightness Temperatures vs. backscatter for ASCAT.

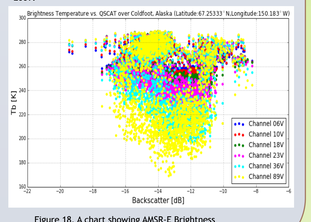

Figure 18. A chart showing AMSR-E Brightness Temperatures vs. backscatter for QuikSCAT.

OBSERVATIONS

As shown by the validation of the SNOTEL data, there is a direct correlation between the soil temperature (freeze/thaw state) and the ASCAT backscatter for both of the transition periods. Thawed conditions are associated with high backscatter values while frozen conditions are associated with low backscatter values. Although the sample here shows only one year of data, a general pattern can also be seen over the entire time period that the data were collected. This is also the case with the CWT data collected over the same station location, which shows significant trends in seasonal freeze/thaw transitions over the five-year period examined. The AMSR-E brightness temperature data that was collected from 2002 to 2011 also supports this.

QuikSCAT data show different relationships. As shown in both the time series dataset and the freeze/thaw detection generated by the CWT, there is less direct correspondence of backscatter with soil freeze/thaw condition.

FUTURE WORK

On-going and future work for this project include development and assessment of integrated land surface freeze/thaw and sea ice melt/ freeze detection algorithms on ASCAT and QuikSCAT This is being carried out as parallel tasks focused on land and ocean domains:

(1) Identification and evaluation of specific freeze/thaw transitional events over the land at selected ground station locations in order to assess land surface transitional events related to the time series backscatter.

(2) Apply these algorithms over the north polar ocean, classifying that domain in terms of (a) open ocean, (b) first year ice, and (c) multi-year ice, and the associated melt /freeze status of these ice types. Data from drift buoy networks in the Arctic Ocean will be used as point-specific validation for these derived products.

The harmonized land-ocean algorithm will be updated to utilize SMAP observations. The SMAP-based north polar dataset will be integrated with the Navy's model to support operational observation of the ice cover in the north polar ocean domain.

REFERENCES

Mortin J., Howell S., Wang L., Derkson C., Svensson G., Graversen R., and Schrøder T., Extending the QuikSCAT record of seasonal melt-freeze transitions over Arctic sea ice using ASCAT Retrieved July 2, 2014, doi: 141 (2014) 214-230

Mortin J., Schrøder T., Hansen A., Holt B., and McDonald K. C., Mapping of seasonal freeze-thaw transitions across the pan-Arctic land and sea ice domains with satellite radar Retrieved July 2, 2014 , doi: 10.1029/2012JC008001

ACKNOWLEDGEMENTS

This research is funded by a grant from the National Aeronautics and Space Administration and is supported by The National Oceanic and Atmospheric Administration - Cooperative Remote Sensing Science and Technology Center (NOAA-CREST)-Cooperative Agreement No: NA11SEC4810004. Portions of this work were performed at the Jet Propulsion Laboratory, California Institute of Technology, under contract to the National Aeronautics and Space Administration. NOAA CREST.